JOURNAL OF COMPUTATIONAL PHYSICS **134,** 122–133 (1997)
ARTICLE NO. CP975677

BGK-Based Scheme for Multicomponent Flow Calculations

Kun Xu

Mathematics Department, Hong Kong University of Science and Technology, Clear Water Bay, Kowloon, Hong Kong
E-mail: makxu@uxmail.ust.hk

Received August 5, 1996; revised December 9, 1996

This paper concerns the extension of the gas-kinetic BGK-type scheme to multicomponent flow calculations. In this new scheme, each component satisfies its individual gas-kinetic BGK equation and the equilibrium states for each component are coupled in space and time to have common temperature and velocity. The particle diffusion in gas mixtures is included naturally in the gas-kinetic model. The current scheme can handle strong shocks and be oscillation-free through the material interface. The scheme guarantees the exact mass conservation for each component and the exact conservation of total momentum and energy in the whole particle system. As a special application, the current scheme is applied to gas vacuum interaction case, where the mass densities for other components are set to zero in the whole domain. The extension of the current approach to three dimensions is straightforward. With the definition of $\varphi = \rho^{(1)} - \rho^{(2)}$ in the two-component gas flow, similar to the level set method we can follow explicitly the time evolution of the material interface ($\varphi = 0$). The numerical results confirm the accuracy and robustness of the BGK-type scheme.

1. INTRODUCTION

The focus of this paper is to solve the Euler equations for two-component gas flow,

$$\begin{pmatrix} \rho^{(1)} \\ \rho^{(2)} \\ \rho U \\ E \end{pmatrix}_t + \begin{pmatrix} \rho^{(1)} U \\ \rho^{(2)} U \\ \rho U^2 + P \\ U(E+P) \end{pmatrix}_x = 0, \tag{1}$$

where $\rho = \rho^{(1)} + \rho^{(2)}$ is the total density, E is the total energy, and U is the average flow velocity. Each component has its specific heat C_{vi} and γ_i. The equation of state is $\varepsilon_i = \rho_i C_{vi} T$ and P is the total pressure. A detailed introduction about multicomponent flow equations can be found in [11]. A straightforward extension of finite volume upwind schemes based on the Riemann solver to the multicomponent flow calculations usually encounters two difficulties: the mass fraction Y and $1 - Y$ may become negative or the pressure distribution may present oscillations through contact discontinuities. In order to reduce these difficulties, many methods have been attempted, such as modifying the flux function [13], introducing nonconservative variables [11], or designing the specific numerical discretization to update Y for certain flow solvers [1]. Currently, hybrid schemes have become popular for multicomponent flow calculations [12]. Based on gas-kinetic theory, many lattice gas methods have also been developed for the studying of multicomponent gas flow [21, 6], specifically for incompressible immiscible flow and phase transition problems [20].

The gas-kinetic scheme for compressible Euler equations has been introduced by Sanders and Prendergast [19], Reitz [18], Pullin [17], Deshpande [4], and Perthame [15]. All the above schemes developed so far are based on the collisionless Boltzmann equation, yielding results which are more diffusive than those obtained from classical high resolution difference schemes. The physical reason and remedy for this is analyzed in a recent work [22].

In this paper, we are interested in extending the well-developed gas-kinetic BGK scheme to solve the multicomponent compressible Euler equations. Each component has its individual gas-kinetic BGK equation; the equilibrium states for each component are coupled through the physical requirements of total momentum and energy conservation in particle collisions. In each time step, the time-dependent gas distribution functions for each component are obtained simultaneously. The current scheme is a natural extension of the BGK-type schemes for one-component gas [16, 23–25]. There are no specific numerical requirements imposed on the material interface in the current scheme in order to get a smooth transition between different components. Basically, each component is regarded as filling up the whole space and the multicomponent gas interactions are formulated in each cell, although the mass density for certain components could probably be zero. Particle transport in gas mixtures is the basic physical behaviour to be described by the gas kinetic theory and the current approach is an initial attempt to capture these phenomena. The outline of this paper is as follows. In Section 2, we introduce the BGK models for two-compo-

0021-9991/97 $25.00

nent gas flow and present the basic numerical discretizations. Section 3 includes standard test cases. The last section is the conclusion.

2. ONE-DIMENSIONAL MULTICOMPONENT BGK SCHEME

The fundamental task in the construction of a finite-volume gas-kinetic scheme for multicomponent flow simulations is to evaluate the time-dependent gas distribution function f for each component at a cell interface, from which the numerical fluxes are evaluated. For two-component gas flow, there are two macroscopic quantities in space x and time t, which are mass $(\rho^{(1)}(x,t), \rho^{(2)}(x,t))$, momentum $(\rho^{(1)}U^{(1)}(x,t), \rho^{(2)}U^{(2)}(x,t))$, and energy $(E^{(1)}(x,t), E^{(2)}(x,t))$ densities, where (1) and (2) refer to the component 1 and component 2 gases, respectively. Generally, these two components have different specific heat ratio $(\gamma^{(1)}, \gamma^{(2)})$. The governing equation for the time evolution of each component is the BGK model [3],

$$\begin{aligned} f_t^{(1)} + uf_x^{(1)} &= (g^{(1)} - f^{(1)})/\tau, \\ f_t^{(2)} + uf_x^{(2)} &= (g^{(2)} - f^{(2)})/\tau, \end{aligned} \tag{2}$$

where $f^{(1)}$ and $f^{(2)}$ are gas distribution functions for components 1 and 2, and $g^{(1)}$ and $g^{(2)}$ are the corresponding equilibrium states which $f^{(1)}$ and $f^{(2)}$ approach. For each component, the equilibrium state is a Maxwellian distribution with the general formulation,

$$g = \rho(\lambda/\pi)^{(K+1)/2}\, e^{-\lambda((u-U)^2+\xi^2)},$$

where λ is the inverse of temperature. $K^{(1)}$ and $K^{(2)}$ are the degree of internal variable ξ in the distribution functions, which are related to the specific heat ratio $\gamma^{(1)}$ and $\gamma^{(2)}$. Under the assumption of equipartition in the particle system, the relations between K and γ for 1D perfect gas are

$$\begin{aligned} K^{(1)} &= (5 - 3\gamma^{(1)})/(\gamma^{(1)} - 1) + 2, \\ K^{(2)} &= (5 - 3\gamma^{(2)})/(\gamma^{(2)} - 1) + 2. \end{aligned}$$

Due to the momentum and energy exchange in particle collisions between two components, $g^{(1)}$ and $g^{(2)}$ in Eq. (2) are not independent functions. As a physical model, it is postulated that $g^{(1)}$ and $g^{(2)}$ have the same temperature and velocity. This assumption of no velocity slip is reasonable only if the density variation between the components is moderate, as is generally the case with two gases. In some situations, the nonequilibrium particle transport in gas mixtures are important, especially when the molecular weights for each component are very different. In these cases, a modified BGK model is necessary [7] and the current scheme can be also extended there.

Instead of individual mass, momentum, and energy conservation in a single component flow, for two-component gas mixtures the compatibility condition is

$$\begin{aligned} &\int [(g^{(1)} - f^{(1)})\phi_\alpha^{(1)} + (g^{(2)} - f^{(2)})\phi_\alpha^{(2)}]\, du\, d\xi = 0, \\ &\alpha = 1, 2, 3, 4, \end{aligned} \tag{3}$$

where

$$\phi_\alpha^{(1)} = (1, 0, u, \tfrac{1}{2}(u^2 + \xi^2))^{\mathrm{T}}$$

and

$$\phi_\alpha^{(2)} = (0, 1, u, \tfrac{1}{2}(u^2 + \xi^2))^{\mathrm{T}}$$

are the moments for individual mass, total momentum, and total energy densities.

Based on Eq. (2) and Eq. (3), from Chapman–Enskog expansion the diffusion equations between the two components can be derived, for example,

$$\begin{aligned} &\frac{\partial \rho^{(1)}}{\partial t} + \frac{\partial(\rho^{(1)}U)}{\partial x} \\ &\quad = \tau \frac{\partial}{\partial x}\left(\frac{\rho^{(2)}}{\rho^{(1)} + \rho^{(2)}} \frac{\partial}{\partial x}\left(\frac{\rho^{(1)}}{2\lambda}\right) - \frac{\rho^{(1)}}{\rho^{(1)} + \rho^{(2)}} \frac{\partial}{\partial x}\left(\frac{\rho^{(2)}}{2\lambda}\right)\right) \end{aligned}$$

and

$$\begin{aligned} &\frac{\partial \rho^{(2)}}{\partial t} + \frac{\partial(\rho^{(2)}U)}{\partial x} \\ &\quad = \tau \frac{\partial}{\partial x}\left(\frac{\rho^{(1)}}{\rho^{(1)} + \rho^{(2)}} \frac{\partial}{\partial x}\left(\frac{\rho^{(2)}}{2\lambda}\right) - \frac{\rho^{(2)}}{\rho^{(1)} + \rho^{(2)}} \frac{\partial}{\partial x}\left(\frac{\rho^{(1)}}{2\lambda}\right)\right). \end{aligned} \tag{4}$$

Here U and λ are the common velocity and temperature in the equilibrium states $g^{(1)}$ and $g^{(2)}$. If the collision time for $f^{(1)}$ and $f^{(2)}$ in Eq. (2) are different, a similar diffusion equation can be derived [3]. Here one point that needs to be emphasized is that the BGK models for multicomponent flow take into account the effects of particle diffusion between different species, and the numerical scheme presented in this section is actually a flow solver to describe these phenomena. So, from the physical point of view, the current scheme is different from those schemes based on the inviscid Euler equations [12, 1] in which the terms on the right-hand sides of Eq. (4) are assumed to be zero. A multicomponent flow solver for the compressible Euler equations (1) corresponds to $\tau \to 0$ in the gas-kinetic de-

scription. However, due to the limited numerical cell size and time step we can never make τ extremely small. For example, in a smooth flow region τ is usually set to the order of $10^{-3}\ \Delta T$, where ΔT is the numerical time step. So, the particle diffusion is unavoidable.

Due to the momentum and energy exchange in particle collisions, the maximum entropy criteria in the particle system require that the equilibrium states $g^{(1)}$ and $g^{(2)}$ have the common velocity and temperature at any points in space and time. So for any given initial macroscopic variables in space and time,

$$\begin{aligned} W^{(1)} &= (\rho^{(1)}, \rho^{(1)}U^{(1)}, E^{(1)})^{\mathrm{T}}, \\ W^{(2)} &= (\rho^{(2)}, \rho^{(2)}U^{(2)}, E^{(2)})^{\mathrm{T}}, \end{aligned} \tag{5}$$

we can construct the corresponding equilibrium states,

$$g^{(1)} = \rho^{(1)}(\lambda_0/\pi)^{(K^{(1)}+1)/2} e^{-\lambda_0((u-U_0)^2+\xi^2)}$$

and

$$g^{(2)} = \rho^{(2)}(\lambda_0/\pi)^{(K^{(2)}+1)/2} e^{-\lambda_0((u-U_0)^2+\xi^2)}, \tag{6}$$

where the common λ_0 and U_0 can be obtained from the conservation requirements,

$$\rho^{(1)}U^{(1)} + \rho^{(2)}U^{(2)} = (\rho^{(1)} + \rho^{(2)})U_0$$

and

$$\begin{aligned} E^{(1)} + E^{(2)} = {} & \frac{\rho^{(1)} + \rho^{(2)}}{2} U_0^2 \\ & + \frac{(K^{(1)}+1)\rho^{(1)} + (K^{(2)}+1)\rho^{(2)}}{4\lambda_0}. \end{aligned} \tag{7}$$

From the above two equations, U_0 and λ_0 can be obtained explicitly,

$$U_0 = \frac{\rho^{(1)}U^{(1)} + \rho^{(2)}U^{(2)}}{\rho^{(1)} + \rho^{(2)}} \tag{8}$$

and

$$\lambda_0 = \frac{1}{4}\frac{(K^{(1)}+1)\rho^{(1)} + (K^{(2)}+1)\rho^{(2)}}{E^{(1)} + E^{(2)} - \frac{1}{2}(\rho^{(1)} + \rho^{(2)})U_0^2}. \tag{9}$$

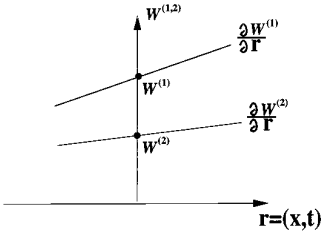

FIG. 1. The linear distributed macroscopic variables $\partial W^{(1,2)}/\partial r$ in $r = (x, t)$.

If both $W^{(1)}$ and $W^{(2)}$ in Eq. (5) are physically realizable states which satisfy

$$(\rho^{(1)} \geq 0, E^{(1)} \geq \tfrac{1}{2}\rho^{(1)}U^{(1)^2})$$

and

$$(\rho^{(2)} \geq 0, E^{(2)} \geq \tfrac{1}{2}\rho^{(2)}U^{(2)^2}),$$

then the value of λ_0 in Eq. (9) is a positive number. As a consequence, the equilibrium states are also physical states with positive temperature and pressure. From thermodynamics, we know that the total entropy in the particle system with the equilibrium states $g^{(1)}$ and $g^{(2)}$ has the largest value for all possible particle distribution functions corresponding to the initial macroscopic states $W^{(1)}$ and $W^{(2)}$ in Eq. (5) where the momentum and energy are exchangeable between different components.

Because of particle collisions, each component relaxes to a local equilibrium state in a time scale of collision time τ. Since the CFL time step used in the current scheme is much larger than the collision time, the exchange of momentum and energy in particle collisions can be finished instantaneously and equalize the temperature and velocity of both components. Therefore, in the numerical point of view at any point in space and time, it is fair enough to modify the individual macroscopic distributions in Eq. (5) to the equilibrium values

$$\begin{aligned} W^{(1)} &= (\rho^{(1)}, \rho^{(1)}U^{(1)}, E^{(1)})^{\mathrm{T}} \\ &= \left(\rho^{(1)}, \rho^{(1)}U_0, \frac{1}{2}\rho^{(1)}\left(U_0^2 + \frac{K^{(1)}+1}{2\lambda_0}\right)\right)^{\mathrm{T}} \end{aligned}$$

and

$$\begin{aligned} W^{(2)} &= (\rho^{(2)}, \rho^{(2)}U^{(2)}, E^{(2)})^{\mathrm{T}} \\ &= \left(\rho^{(2)}, \rho^{(2)}U_0, \frac{1}{2}\rho^{(2)}\left(U_0^2 + \frac{K^{(2)}+1}{2\lambda_0}\right)\right)^{\mathrm{T}}. \end{aligned} \tag{10}$$

The equilibrium states $g^{(1)}$ and $g^{(2)}$ are coupled with the common temperature and velocity at any point in space and time, $r = (x, t)$; their slopes in r should also be related to each other. As shown in Fig. 1, once we know $W^{(1)}$, $W^{(2)}$, and their linear slopes for the macroscopic variables,

$$W^{(1)} + \frac{\partial W^{(1)}}{\partial r} r = W^{(1)} + \left(\frac{\partial \rho^{(1)}}{\partial r}, \frac{\partial \rho^{(1)} U^{(1)}}{\partial r}, \frac{\partial E^{(1)}}{\partial r} \right)^{\mathrm{T}} r$$

and

$$W^{(2)} + \frac{\partial W^{(2)}}{\partial r} r = W^{(2)} + \left(\frac{\partial \rho^{(2)}}{\partial r}, \frac{\partial \rho^{(2)} U^{(2)}}{\partial r}, \frac{\partial E^{(2)}}{\partial r} \right)^{\mathrm{T}} r,$$

we can construct the equivalent gas distribution functions $g^{(1)}$ and $g^{(2)}$, and their slopes $(m^{(1)}, n^{(1)}, \rho^{(1)})$ and $(m^{(2)}, n^{(2)}, \rho^{(2)})$ in the equivalent expansion of Maxwellian distribution functions at the same point,

$$\begin{aligned} &[1 + (m^{(1)} + n^{(1)} u + p^{(1)}(u^2 + \xi^2))r]\, g^{(1)}, \\ &[1 + (m^{(2)} + n^{(2)} u + p^{(2)}(u^2 + \xi^2))r]\, g^{(2)}. \end{aligned} \tag{11}$$

Due to the relations between $g^{(1)}$ and $g^{(2)}$ in Eq. (6), the values of $(m^{(1,2)}, n^{(1,2)}, p^{(1,2)})$ in Eq. (11) are not totally independent variables. Since $n^{(1)}, p^{(1)}, n^{(2)}, p^{(2)}$ depend only on the rth-derivative of U_0 and λ_0, the common velocity and temperature locally in space and time require

$$n \equiv n^{(1)} = n^{(2)}, \quad p \equiv p^{(1)} = p^{(2)}.$$

So, the connections between macroscopic and microscopic distributions can be reduced to

$$\begin{aligned} &\begin{pmatrix} \dfrac{\partial \rho^{(1)}}{\partial r} \\ \dfrac{\partial \rho^{(2)}}{\partial r} \\ \dfrac{\partial (\rho^{(1)} U^{(1)} + \rho^{(2)} U^{(2)})}{\partial r} \\ \dfrac{\partial (E^{(1)} + E^{(2)})}{\partial r} \end{pmatrix} \equiv \begin{pmatrix} \omega_1 \\ \omega_2 \\ \omega_3 \\ \omega_4 \end{pmatrix} \\ &= \int [(m^{(1)} + nu + p(u^2 + \xi^2)) g^{(1)} \phi_\alpha^{(1)} \\ &\quad + (m^{(2)} + nu + p(u^2 + \xi^2)) g^{(2)} \phi_\alpha^{(2)}]\, du\, d\xi. \end{aligned} \tag{12}$$

The above four equations uniquely determine the four unknowns $(m^{(1)}, m^{(2)}, n, p)$ and the solutions can be obtained in the following: Define

$$\Pi_1 = \omega_3 - U_0(\omega_1 + \omega_2)$$

$$\Pi_2 = 2\omega_4 - \left(U_0^2 + \frac{K^{(1)} + 1}{2\lambda_0} \right) \omega_1 - \left(U_0^2 + \frac{K^{(2)} + 1}{2\lambda_0} \right) \omega_2.$$

The solutions of Eq. (12) are

$$p = \frac{2\lambda_0^2 (\Pi_2 - 2U_0 \Pi_1)}{(K^{(1)} + 1)\rho^{(1)} + (K^{(2)} + 1)\rho^{(2)}}$$

$$n = \frac{2\lambda_0}{\rho^{(1)} + \rho^{(2)}} \left(\Pi_1 - \frac{(\rho^{(1)} + \rho^{(2)}) U_0}{\lambda_0} p \right)$$

$$m^{(1)} = \frac{1}{\rho^{(1)}} \left(\omega_1 - \rho^{(1)} U_0 n - \rho^{(1)} \left(U_0^2 + \frac{K^{(1)} + 1}{2\lambda_0} \right) p \right)$$

$$m^{(2)} = \frac{1}{\rho^{(2)}} \left(\omega_2 - \rho^{(2)} U_0 n - \rho^{(2)} \left(U_0^2 + \frac{K^{(2)} + 1}{2\lambda_0} \right) p \right).$$

The above solutions will be used several times in the current two-component BGK solver to obtain both spatial and temporal variations of the particle distribution functions.

In the numerical scheme, the space is divided into cells. For each cell j, the cell center is located at x_j and the cell interfaces are $x_{j-1/2}$ and $x_{j+1/2}$. The cell-averaged macroscopic variables are denoted as $W_j^{(1)}$ and $W_j^{(2)}$, for the mass, momentum, and energy. In order to update the cell-averaged values $W_j^{(1,2)}$, we need to get the numerical fluxes across the cell interface. These fluxes are determined from the time-dependent gas distribution functions. The gas distribution function for each component at a cell interface can be obtained from the integral solution of the BGK model,

$$\begin{aligned} f^{(1)}(x_{j+1/2}, t, u, \xi) = &\frac{1}{\tau} \int_0^t g^{(1)}(x', t', u, \xi) e^{-(t-t')/\tau}\, dt' \\ &+ e^{-t/\tau} f_0^{(1)}(x_{j+1/2} - ut) \end{aligned} \tag{13}$$

for component 1, and

$$\begin{aligned} f^{(2)}(x_{j+1/2}, t, u, \xi) = &\frac{1}{\tau} \int_0^t g^{(2)}(x', t', u, \xi) e^{-(t-t')/\tau}\, dt' \\ &+ e^{-t/\tau} f_0^{(2)}(x_{j+1/2} - ut) \end{aligned} \tag{14}$$

for component 2, where $x_{j+1/2}$ is the cell interface and $x' = x_{j+1/2} - u(t - t')$ the particle trajectory. There are four unknowns in Eq. (13) and Eq. (14). Two of them are initial gas distribution functions $f_0^{(1)}$ and $f_0^{(2)}$ at the beginning of each time step $t = 0$, and the others are $g^{(1)}$ and $g^{(2)}$ in both space and time locally around $(x_{j+1/2}, t = 0)$. In order to obtain all these unknowns, the BGK scheme is summarized as follows.

(1) Modify the initial cell average conservative variables $W_j^{(1,2)}$ in each cell j to the equilibrium values according to Eq. (10) where the equilibrium velocity and temperature in each cell are obtained using Eq. (8) and Eq. (9). Then, apply TVD, ENO, or LED [8–10] techniques to

interpolate the equilibrium conservative variables $W_j^{(1,2)}$ in each cell j to get the reconstructed initial data

$$W_j^{(1,2)}(x) = W_j^{(1,2)} + \frac{W_j^{(1,2)}(x_{j+1/2}) - W_j^{(1,2)}(x_{j-1/2})}{x_{j+1/2} - x_{j-1/2}}(x - x_j) \quad \text{for } x\varepsilon[x_{j-1/2}, x_{j+1/2}]. \tag{15}$$

In order to get the left and right states $(W_j^{(1,2)}(x_{j-1/2}), W_j^{(1,2)}(x_{j+1/2}))$, nonlinear limiters should be used.

(2) Based on states $(W_j^{(1,2)}(x_{j+1/2}), W_{j+1}^{(1,2)}(x_{j+1/2}))$, use Eq. (8) and Eq. (9) on both sides of the cell interface $x_{j+1/2}$ to evaluate the equilibrium velocities U_0^l, U_0^r and temperatures λ_0^l, λ_0^r, and modify these reconstructed data to the new values according to Eq. (10), which are denoted as

$$\tilde{W}_j^{(1,2)}(x_{j+1/2}), \quad \tilde{W}_{j+1}^{(1,2)}(x_{j+1/2}). \tag{16}$$

Then, connect the above values in Eq. (16) to the cell-centered values in Eq. (15),

$$W_j^{(1,2)}(x_j), \quad W_{j+1}^{(1,2)}(x_{j+1}), \tag{17}$$

to get the linear slopes of mass, momentum, and energy densities for each component on both sides of a cell interface,

$$\frac{\tilde{W}_j^{(1,2)}(x_{j+1/2}) - W_j^{(1,2)}(x_j)}{x_{j+1/2} - x_j}, \quad \frac{W_{j+1}^{(1,2)}(x_{j+1}) - \tilde{W}_{j+1}^{(1,2)}(x_{j+1/2})}{x_{j+1} - x_{j+1/2}}. \tag{18}$$

In order to translate the above macroscopic flow distributions into the equivalent microscopic gas distribution functions, we construct the initial distribution functions $f_0^{(1)}$ and $f_0^{(2)}$ in Eq. (13) and Eq. (14) as

$$f_0^{(1)} = \begin{cases} (1 + a_l^{(1)}(x - x_{j+1/2}))g_l^{(1)}, & x \le x_{j+1/2}, \\ (1 + a_r^{(1)}(x - x_{j+1/2}))g_r^{(1)}, & x \ge x_{j+1/2}, \end{cases} \tag{19}$$

for component 1, and

$$f_0^{(2)} = \begin{cases} (1 + a_l^{(2)}(x - x_{j+1/2}))g_l^{(2)}, & x \le x_{j+1/2}, \\ (1 + a_r^{(2)}(x - x_{j+1/2}))g_r^{(2)}, & x \ge x_{j+1/2}, \end{cases} \tag{20}$$

for component 2. And $g_l^{(1)}$, $g_l^{(2)}$ can be obtained from the macroscopic densities $\tilde{W}_j^{(1,2)}(x_{j+1/2})$ in Eq. (16), which are

$$g_l^{(1)} = \rho_l^{(1)}(\lambda_0^l/\pi)^{(K^{(1)}+1)/2} e^{-\lambda_0^l((u-U_0^l)^2+\xi^2)}$$

and

$$g_l^{(2)} = \rho_l^{(2)}(\lambda_0^l/\pi)^{(K^{(2)}+1)/2} e^{-\lambda_0^l((u-U_0^l)^2+\xi^2)}. \tag{21}$$

Similarly, $g_r^{(1)}$ and $g_r^{(2)}$ can be found from $\tilde{W}_{j+1}^{(1,2)}(x_{j+1/2})$ in Eq. (16),

$$g_r^{(1)} = \rho_r^{(1)}(\lambda_0^r/\pi)^{(K^{(1)}+1)/2} e^{-\lambda_0^r((u-U_0^r)^2+\xi^2)}$$

and

$$g_r^{(2)} = \rho_r^{(2)}(\lambda_0^r/\pi)^{(K^{(2)}+1)/2} e^{-\lambda_0^r((u-U_0^r)^2+\xi^2)}. \tag{22}$$

The terms $a_{l,r}^{(1,2)}$ in Eq. (19) and Eq. (20) are composed of

$$a_{l,r}^{(1,2)} = m_{l,r}^{(1,2)} + n_{l,r}u + p_{l,r}(u^2 + \xi^2),$$

which can be determined on both sides of a cell interface in terms of the slopes of macroscopic variables in Eq. (18) by using the techniques for solving Eq. (12) with $r = x$. At this point, all the parameters in Eq. (19) and Eq. (20) for the initial gas distribution functions at the beginning of each time step are determined from the initial reconstructed macroscopic distributions.

(3) Assume the equilibrium states in Eq. (13) and Eq. (14) around $(x_{j+1/2}, t = 0)$ as

$$g^{(1)} = (1 + (1 - \mathrm{H}[x - x_{j+1/2}])(x - x_{j+1/2})\overline{a}_l^{(1)} + \mathrm{H}[x - x_{j+1/2}](x - x_{j+1/2})\overline{a}_r^{(1)} + \overline{A}^{(1)}t)g_0^{(1)} \tag{23}$$

and

$$g^{(2)} = (1 + (1 - \mathrm{H}[x - x_{j+1/2}])(x - x_{j+1/2})\overline{a}_l^{(2)} + \mathrm{H}[x - x_{j+1/2}](x - x_{j+1/2})\overline{a}_r^{(2)} + \overline{A}^{(2)}t)g_0^{(2)}, \tag{24}$$

where H is the heaviside function. And $g_0^{(1)}$ and $g_0^{(2)}$ are the initial equilibrium states located exactly at the cell interface,

$$g_0^{(1)} = \rho_0^{(1)}(\lambda_0/\pi)^{(K^{(1)}+1)/2} e^{-\lambda_0((u-U_0)^2+\xi^2)}$$

and

$$g_0^{(2)} = \rho_0^{(2)}(\lambda_0/\pi)^{(K^{(2)}+1)/2} e^{-\lambda_0((u-U_0)^2+\xi^2)}. \tag{25}$$

The parameters $\overline{a}_{l,r}^{(1,2)}$ and $\overline{A}^{(1,2)}$ have the forms

$$\overline{a}_{l,r}^{(1,2)} = \overline{m}_{l,r}^{(1,2)} + \overline{n}_{l,r}u + \overline{p}_{l,r}(u^2 + \xi^2),$$
$$\overline{A}^{(1,2)} = \overline{A}_a^{(1,2)} + \overline{A}_b u + \overline{A}_c(u^2 + \xi^2).$$

And $g_0^{(1)}$ and $g_0^{(2)}$ in Eqs. (23) and (24) can be obtained self-consistently by taking the limits of $(t \to 0)$ in Eq. (13) and Eq. (14) and applying the compatibility condition at $(x = x_{j+1/2}, t = 0)$, which gives

$$\begin{pmatrix} \rho_0^{(1)} \\ \rho_0^{(2)} \\ (\rho_0^{(1)} + \rho_0^{(2)})U_0 \\ E_0^{(1)} + E_0^{(2)} \end{pmatrix} \equiv \int (g_0^{(1)}\phi_\alpha^{(1)} + g_0^{(2)}\phi_\alpha^{(2)})\, du\, d\xi \tag{26}$$

$$= \int [(\mathrm{H}[u]g_l^{(1)} + (1 - \mathrm{H}[u])g_r^{(1)})\phi_\alpha^{(1)} + (g_l^{(2)}\mathrm{H}[u] + g_r^{(2)}(1 - \mathrm{H}[u]))\phi_\alpha^{(2)}]\, du\, d\xi.$$

By using $g_{l,r}^{(1,2)}$ in Eq. (21) and Eq. (22), the right-hand side of Eq. (26) can be evaluated explicitly. Therefore, $\rho_0^{(1)}$, $\rho_0^{(2)}$, λ_0, and U_0 in Eq. (25) can be obtained from Eq. (26). As a result, $g_0^{(1)}$ and $g_0^{(2)}$ are totally determined. Then, connecting the macroscopic variables,

$$W_0^{(1)} = (\rho_0^{(1)}, \rho_0^{(1)}U_0, E_0^{(1)}), \quad W_0^{(2)} = (\rho_0^{(2)}, \rho_0^{(2)}U_0, E_0^{(2)}),$$

at the cell interface to the cell-centered values in Eq. (17) on both sides, we can obtain the slopes for the macroscopic variables,

$$\frac{W_0^{(1,2)} - W_j^{(1,2)}(x_j)}{x_{j+1/2} - x_j}, \quad \frac{W_{j+1}^{(1,2)}(x_{j+1}) - W_0^{(1,2)}}{x_{j+1} - x_{j+1/2}},$$

from which $\overline{a}_l^{(1)}$ and $\overline{a}_l^{(2)}$ on the left side and $\overline{a}_r^{(1)}$ and $\overline{a}_r^{(2)}$ on the right side in Eq. (23) and Eq. (24) can be obtained by using the same techniques for solving Eq. (12) with $r = x$. At this point, there are still two unknowns, $\overline{A}^{(1,2)}$, for the time variation parts of the gas distribution functions in Eq. (23) and Eq. (24).

(4) Substituting Eq. (23), Eq. (24), Eq. (19), and Eq. (20) into the integral solutions Eq. (13) and Eq. (14), we get

$$\begin{aligned} f^{(1)}(x_{j+1/2}, t, u, \xi) = {} & (1 - e^{-t/\tau})g_0^{(1)} \\ & + (\tau(-1 + e^{-t/\tau}) + te^{-t/\tau}) \\ & \quad (\overline{a}_l^{(1)}\mathrm{H}[u] + \overline{a}_r^{(1)}(1 - \mathrm{H}[u]))ug_0^{(1)} \\ & + \tau(t/\tau - 1 + e^{-t/\tau})\overline{A}^{(1)}g_0^{(1)} \\ & + e^{-t/\tau}((1 - uta_l^{(1)})\mathrm{H}[u]g_l^{(1)} \\ & + (1 - uta_r^{(1)})(1 - \mathrm{H}[u])g_r^{(1)}) \end{aligned} \tag{27}$$

and

$$\begin{aligned} f^{(2)}(x_{j+1/2}, t, u, \xi) = {} & (1 - e^{-t/\tau})g_0^{(2)} \\ & + (\tau(-1 + e^{-t/\tau}) + te^{-t/\tau}) \\ & \quad (\overline{a}_l^{(2)}\mathrm{H}[u] + \overline{a}_r^{(2)}(1 - \mathrm{H}[u]))ug_0^{(2)} \\ & + \tau(t/\tau - 1 + e^{-t/\tau})\overline{A}^{(2)}g_0^{(2)} \\ & + e^{-t/\tau}((1 - uta_l^{(2)})\mathrm{H}[u]g_l^{(2)} \\ & + (1 - uta_r^{(2)})(1 - \mathrm{H}[u])g_r^{(2)}). \end{aligned} \tag{28}$$

In order to evaluate the unknowns $\overline{A}^{(1,2)}$ in the above two equations, we can use the compatibility condition at the cell interface $x_{j+1/2}$ on the whole CFL time step ΔT,

$$\int_0^{\Delta T} \int [(g^{(1)} - f^{(1)})\phi_\alpha^{(1)} + (g^{(2)} - f^{(2)})\phi_\alpha^{(2)}]\, du\, d\xi\, dt = 0,$$

from which we can get

$$\begin{aligned} & \int [g_0^{(1)}\overline{A}^{(1)}\phi_\alpha^{(1)} + g_0^{(2)}\overline{A}^{(2)}\phi_\alpha^{(2)}]\, du\, d\xi \\ & = [(\overline{A}_a^{(1)} + \overline{A}_b u + \overline{A}_c(u^2 + \xi^2))g_0^{(1)}\phi_\alpha^{(1)} \\ & \quad + (\overline{A}_a^{(2)} + \overline{A}_b u + \overline{A}_c(u^2 + \xi^2))g_0^{(2)}\phi_\alpha^{(2)}]\, du\, d\xi \\ & \equiv \begin{pmatrix} \dfrac{\partial \rho^{(1)}}{\partial t} \\ \dfrac{\partial \rho^{(2)}}{\partial t} \\ \dfrac{\partial(\rho^{(1)}U^{(1)} + \rho^{(2)}U^{(2)})}{\partial t} \\ \dfrac{\partial(E^{(1)} + E^{(2)})}{\partial t} \end{pmatrix} \end{aligned} \tag{29}$$

$$\begin{aligned} = {} & \frac{1}{\Gamma_0}\int [\Gamma_1 g_0^{(1)} + \Gamma_2 u(\overline{a}_l^{(1)}\mathrm{H}[u] + \overline{a}_r^{(1)}(1 - \mathrm{H}[u]))g_0^{(1)} \\ & + \Gamma_3(\mathrm{H}[u]g_l^{(1)} + (1 - \mathrm{H}[u])g_r^{(1)}) \\ & + \Gamma_4 u(a_l^{(1)}\mathrm{H}[u]g_l^{(1)} + a_r^{(1)}(1 - \mathrm{H}[u])g_r^{(1)})]\phi_\alpha^{(1)}\, du\, d\xi \\ & + [\Gamma_1 g_0^{(2)} + \Gamma_2 u(\overline{a}_l^{(2)}\mathrm{H}[u] + \overline{a}_r^{(2)}(1 - \mathrm{H}[u]))g_0^{(2)} \\ & + \Gamma_3(\mathrm{H}[u]g_l^{(2)} + (1 - \mathrm{H}[u])g_r^{(2)}) \\ & + \Gamma_4 u(\overline{a}_l^{(2)}\mathrm{H}[u]g_l^{(2)} + a_r^{(2)}(1 - \mathrm{H}[u])g_r^{(2)})]\phi_\alpha^{(2)}\, du\, d\xi, \end{aligned}$$

where

$$\begin{aligned} \Gamma_0 &= \Delta T - \tau(1 - e^{-\Delta T/\tau}), \\ \Gamma_1 &= -(1 - e^{-\Delta T/\tau}), \\ \Gamma_2 &= (-T + 2\tau(1 - e^{-\Delta T/\tau}) - \Delta T e^{-\Delta t/\tau}), \\ \Gamma_3 &= (1 - e^{-\Delta T/\tau}), \\ \Gamma_4 &= (\Delta T e^{-\Delta T/\tau} - \tau(1 - e^{-\Delta T/\tau})). \end{aligned}$$

Since all terms on the right-hand side of Eq. (29) are known and the integral can be evaluated explicitly, the coefficients $(\overline{A}_a^{(1,2)}, \overline{A}_b, \overline{A}_c)$ can be determined from Eq. (29) by using the techniques for solving Eq. (12) with $r = t$.

(5) Finally the time-dependent numerical fluxes for component 1 and component 2 gases across a cell interface can be obtained by taking the moments of the individual distribution function $f^{(1)}$ and $f^{(2)}$ in Eq. (27) and Eq. (28) separately, which are

$$\begin{pmatrix} \mathscr{F}_{\rho^{(1)}} \\ 0 \\ \mathscr{F}_{\rho^{(1)}U^{(1)}} \\ \mathscr{F}_{E^{(1)}} \end{pmatrix}_{j+1/2} = \int u\phi_\alpha^{(1)} f^{(1)}(x_{j+1/2}, t, u, \xi)\, du\, d\xi$$

and

$$\begin{pmatrix} 0 \\ \mathscr{F}_{\rho^{(2)}} \\ \mathscr{F}_{\rho^{(2)}U^{(2)}} \\ \mathscr{F}_{E^{(2)}} \end{pmatrix}_{j+1/2} = \int u\phi_\alpha^{(2)} f^{(2)}(x_{j+1/2}, t, u, \xi)\, du\, d\xi.$$

Then, integrating the above equations in a whole time step ΔT, we can get the total mass, momentum, and energy transports for each component, from which the flow variables in each cell get updated. For the next time step, we go back to step (1) and repeat all the above steps.

3. NUMERICAL EXAMPLES

Three shock tube test cases are presented in this section to validate the current approach for the multicomponent flow calculations. In all calculations, the length of the numerical domain is equal to 100 and each cell size is $\Delta x = 1$. Different from any other approaches [11, 1], in our scheme the van Leer's limiter is used for the reconstruction of *conservative* variables for each component in each cell directly without using any specific numerical requirements of smooth material interface. The time step is determined by the common CFL condition, where the CFL number is equal to 0.65. The collision time τ is a local constant, which is set to

$$\tau = 0.1\,\Delta T \frac{\sqrt{\lambda_0}}{\rho_0} + \Delta T \frac{|P_l - P_r|}{P_l + P_r},$$

where (λ_0, ρ_0) are the temperature and density of $g_0^{(1,2)}$ in Eq. (25) and (P_l, P_r) are the corresponding pressure terms in the left $g_l^{(1,2)}$ and right states $g_r^{(1,2)}$ in Eq. (21) and Eq. (22), where the pressure P is related to (ρ, λ) through $P = \rho/2\lambda$. The first term in the collision time corresponds to the physical viscosity and the second one accounts for the artificial viscosity. The artificial one guarantees that the real gas distribution function will stay on the non-Maxwellian state in the nonequilibrium flow region.

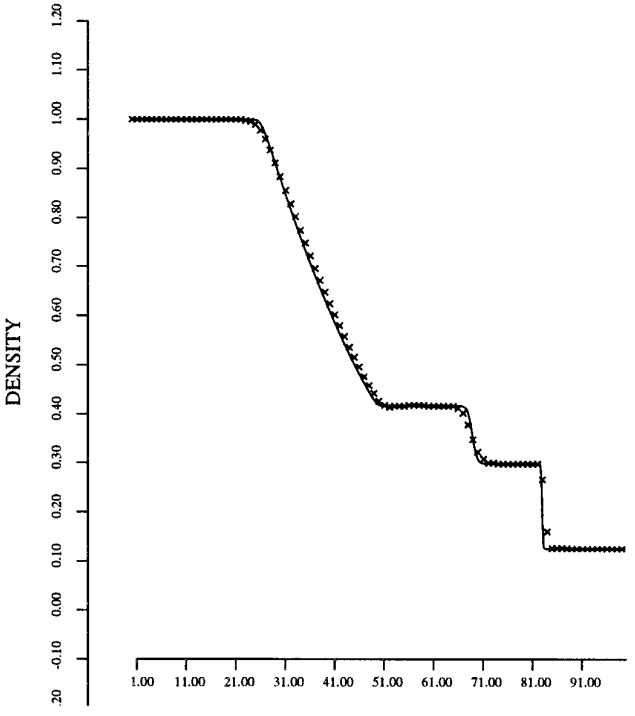

FIG. 2. Total density distribution $(\rho^{(1)} + \rho^{(2)})$.

Case 1. The first test case is taken from [11, 13], and the initial condition is

$$W_L = (\rho_L, \rho_L U_L, E_L, \gamma_L) = (1.0, 0.0, 2.5, 1.4)$$
$$W_R = (\rho_R, \rho_R U_R, E_R, \gamma_R) = (0.125, 0.0, 0.5, 1.2).$$

In this calculation, the initial discontinuity is located at $x = 50$. The simulation results are shown in Figs. 2–4 for total density $(\rho^{(1)} + \rho^{(2)})$, pressure, and velocity. In all these figures, the solid lines are the curves obtained from 400 grid points with the same BGK scheme. The pressure and velocity are very smooth across the material interface, although all conservative variables are used in the initial reconstruction. The pressure distribution in Fig. 3 is obtained as a passive variable from the conservative variables at the output time. Figure 5 presents the average γ in each cell which is defined as $\gamma = (K + 3)/(K + 1)$ and the average K is $K = (\rho^{(1)}K^{(1)} + \rho^{(2)}K^{(2)})/(\rho^{(1)} + \rho^{(2)})$. Figure 6 and Fig. 7 are the individual mass densities $\rho^{(1)}$ and $\rho^{(2)}$ for each component. Since we follow the time evolution

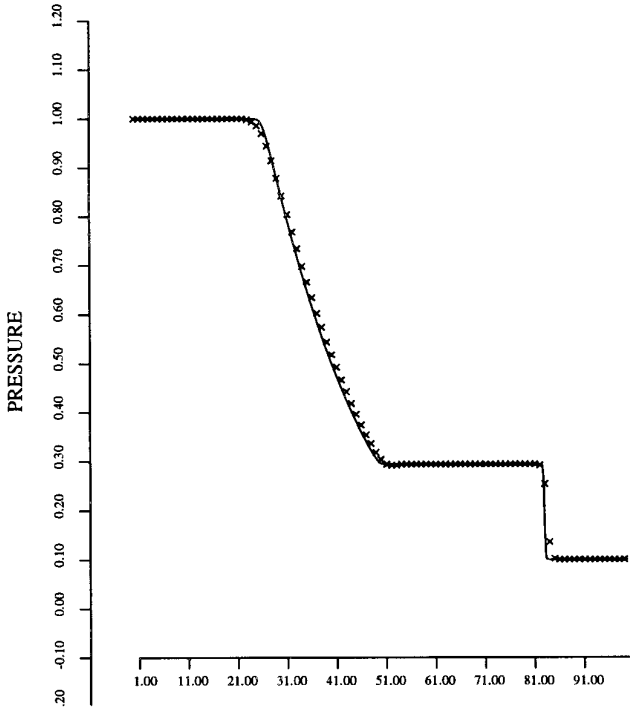

FIG. 3. Pressure distribution.

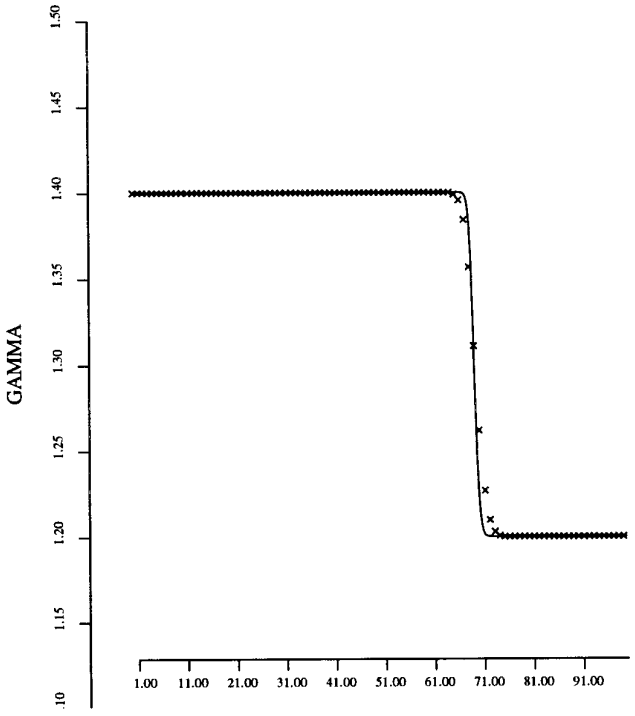

FIG. 5. γ distribution.

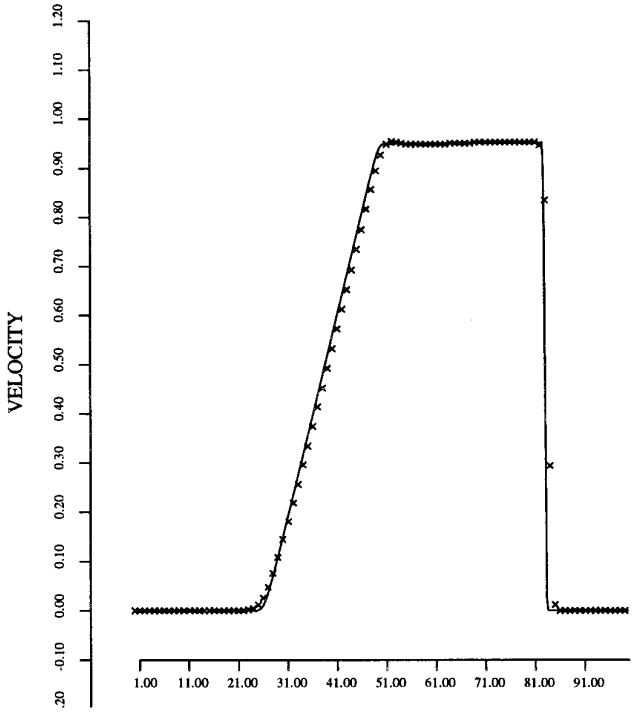

FIG. 4. Velocity distribution.

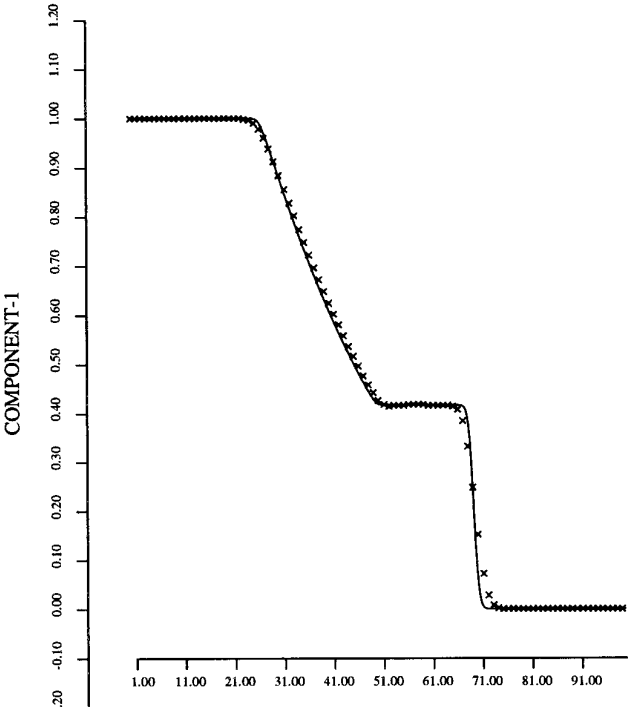

FIG. 6. Density $\rho^{(1)}$ distribution.

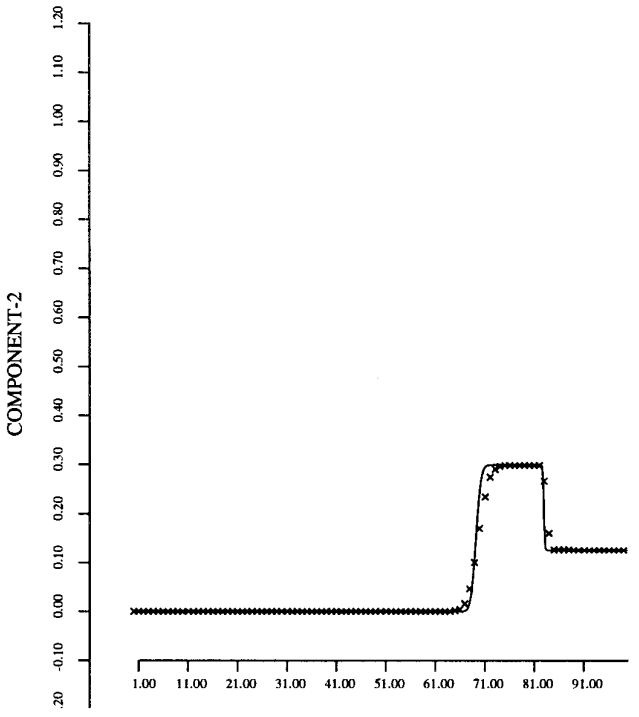

FIG. 7. Density $\rho^{(2)}$ distribution.

of each component explicitly, the total mass for each component is precisely conserved. If there were no momentum and energy exchange between two components through particle collisions, the physical problem would become the one in which each component expands into the vacuum, and the final results will be totally different from these results shown above. Also, as shown in Fig. 6 and Fig. 7, both $\rho^{(1)}$ and $\rho^{(2)}$ around the material interface reduce from certain values to zero. If we define $\varphi = \rho^{(1)} - \rho^{(2)}$, according to the sign of φ, we can know in each cell which component the gas is mostly composed of. If we define $\varphi = 0$ as the material interface, the function φ will be a variable similar to the level set function [14]. However, φ is updated in our scheme according to the different physical model and the distribution of φ can be used as a measure of particle diffusions.

Case 2. The second test case is taken from Abgrall's recent paper [1] with the initial data

$$W_L = (\rho_L, \rho_L U_L, E_L, \gamma_L) = (14.54903, 0.0, 2.9 \times 10^7, 1.67),$$
$$W_R = (\rho_R, \rho_R U_R, E_R, \gamma_R) = (1.16355, 0.0, 2.5 \times 10^5, 1.40).$$

This example is interesting and very difficult for multicomponent flow solvers. One hundred mesh points are used for our BGK solver. Figures 8–13 show the total mass density ($\rho^{(1)} + \rho^{(2)}$), pressure, velocity, γ, $\rho^{(1)}$, and $\rho^{(2)}$ separately, where the solid lines are obtained from the same scheme with 400 grid points. The velocity and pressure are very smooth at the material interface, but a small wiggle appears at the end of the rarefaction wave. It seems that this wiggle is not caused by the current techniques designed specifically for the two-component flow solver. Even for the single component BGK solver, if the initial data has extremely large density and pressure jump, a similar wiggle usually appears. This mechanism of the appearance of wiggle is inherent to the finite volume method.

For the test case of shock–bubble interaction presented in [1], the current scheme has some difficulties. Because the gas-kinetic scheme is a scheme designed to describe the advection–diffusion equation, it can never keep a contact discontinuity sharp and stationary. The physical diffusion and heat conduction due to particle transport in gases will naturally smear the contact discontinuity. So, before the shock interacts with the bubble, the bubble surface has already been smeared in a few cells and the thickness depends on the collision time. It seems that for the shock–interface interaction cases, the carefully designed schemes based on the approximate Riemann solver should be useful, at least in the 1D case, since these schemes could perfectly keep the contact material interface sharp before the contact becomes involved in the interactions with

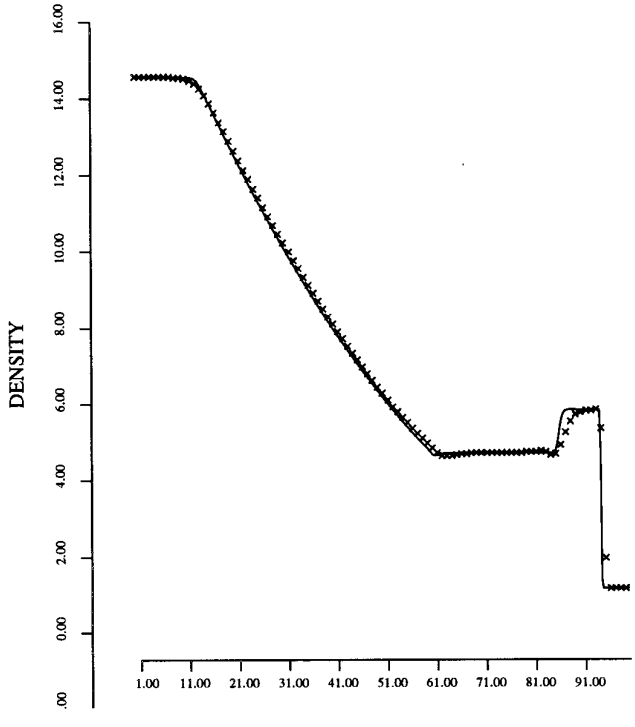

FIG. 8. Total density distribution ($\rho^{(1)} + \rho^{(2)}$).

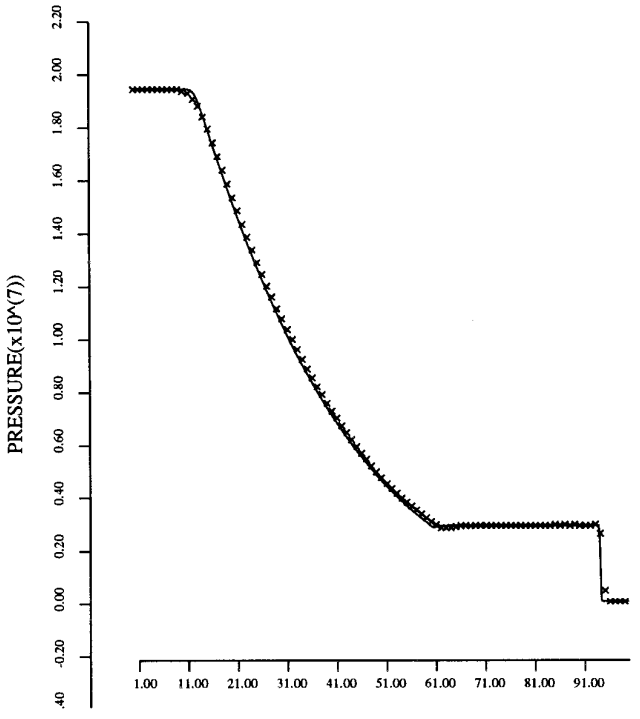

FIG. 9. Pressure distribution.

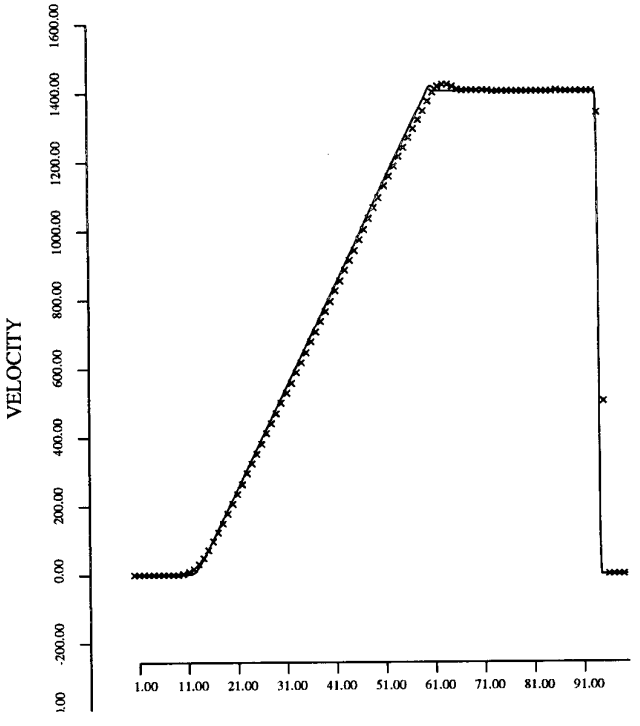

FIG. 10. Velocity distribution.

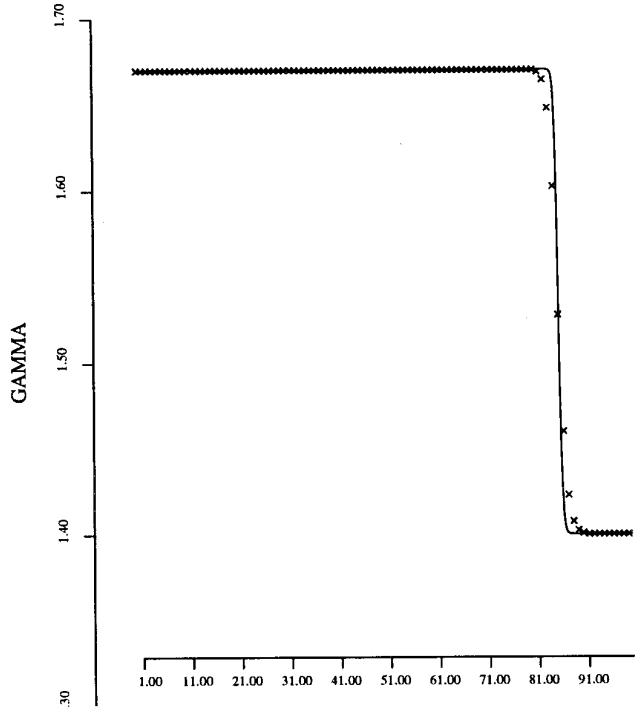

FIG. 11. γ distribution.

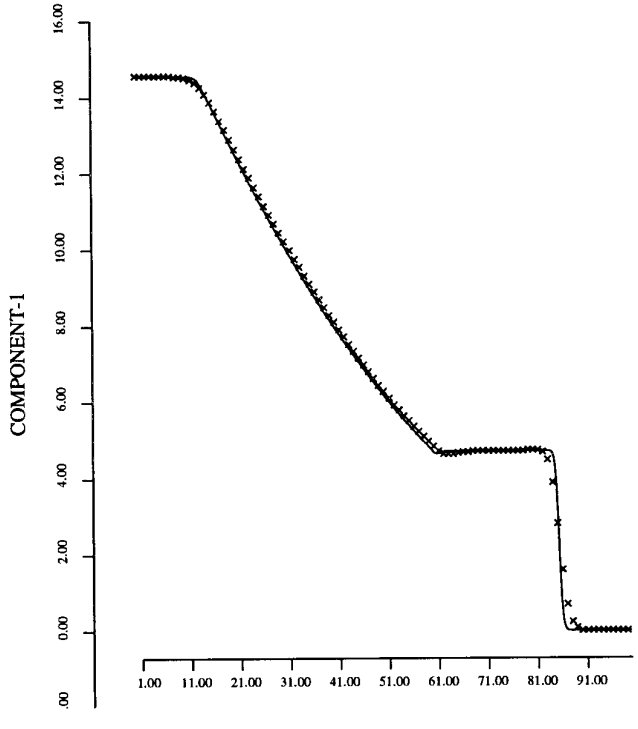

FIG. 12. Density $\rho^{(1)}$ distribution.

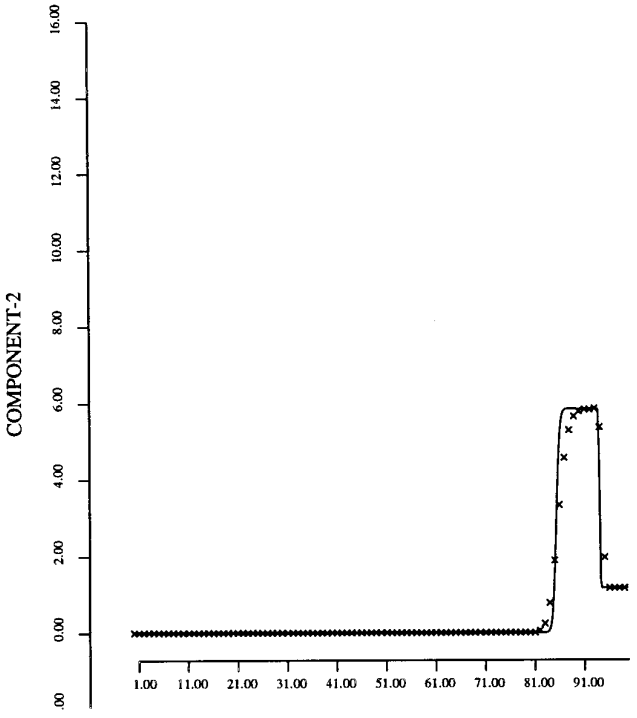

FIG. 13. Density $\rho^{(2)}$ distribution.

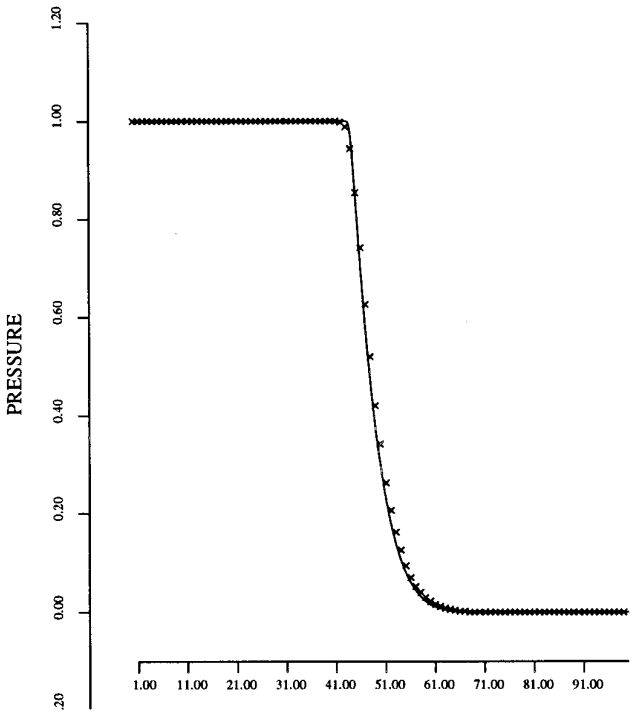

FIG. 15. Pressure distribution.

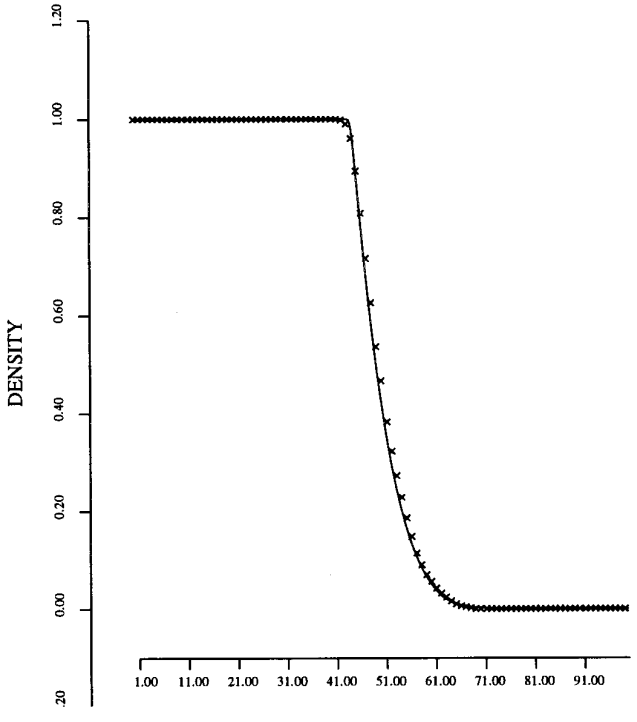

FIG. 14. Density distribution $\rho^{(1)}$.

shocks. However, for the general cases where the initial bubble surface is located in the middle of a numerical cell, the ability of any shock-capturing schemes to keep the stationary material interface sharp and free of wiggles is doubtful. For these applications where the advection–diffusion phenomena are important (not purely artificial diffusion), such as pollutant propagation and turbulent mixing layer, the gas-kinetic scheme will be very helpful and the BGK models could naturally describe this kind of physical phenomena [21]. Another good application for the current scheme is that it can be applied to the gas–vacuum expansion problem, such as to study the interstellar medium and confined plasma. It is well known, the Riemann solver has great difficulty in handling the gas–vacuum expansion case, where the density and temperature easily become negative, especially for the approximate Riemann solver [5].

Case 3. As a third case, we test the gas–vacuum expansion phenomena with the initial data,

$$W_L = (\rho_L, \rho_L U_L, E_L, \gamma_L) = (1.0, 0.0, 2.5, 1.4)$$
$$W_R = (\rho_R, \rho_R U_R, E_R, \gamma_R) = (0.0, 0.0, 0.0, 0.0),$$

where all flow variables on the right-hand side are totally zero. One hundred grid points are used here. The simulation results are shown in Figs. 14–15 for the density and

pressure distributions for the one-component gas. The solid lines are obtained from the same scheme with 400 grid points. Comparing Fig. 14 and Fig. 6, we can observe clearly the effects of particle collisions between different components and the effects of dynamical coupling in the two-component gas evolution.

4. CONCLUSION

In this paper, we have developed a new scheme based on the gas-kinetic equation for multicomponent flow calculations. The scheme is based on the BGK model for each component, from which the advection–diffusion equation can be derived [3]. Since we have followed the time-evolution of the distribution function for each component explicitly, the total mass for each component is precisely conserved. The current scheme can be also extended to the three-dimensional case without major modifications. Capturing the particle diffusion process in multicomponent gas flows by numerical methods is a tough problem; nevertheless the current approach is a starting point in this direction. We believe that the gas-kinetic scheme will be quite promising to describe the transport phenomena.

ACKNOWLEDGMENTS

I thank Professors A. Jameson and L. Martinelli at Princeton University for their support and encouragement in this study and the unknown referees for their helpful comments on our earlier manuscript. This research is supported by Grant URI/AFOSR F49620-93-1-0427 and the Research Grant Council of Hong Kong by Grant DAG 96/97.

REFERENCES

1. R. Abgrall, How to prevent pressure oscillations in multicomponent flow calculations: A quasi conservative approach, *J. Comput. Phys.* **125,** 150 (1996).
2. P. L. Bhatnagar, E. P. Gross, and M. Krook, A model for collision processes in gases I: Small amplitude processes in charged and neutral one-component systems, *Phys. Rev.* **94,** 511 (1954).
3. S. Chapman and T. G. Cowling, *The Mathematical Theory of Non-Uniform Gases,* 3rd ed. (Cambridge Univ. Press, Cambridge, 1990).
4. S. M. Deshpande, *A Second Order Accurate, Kinetic-Theory Based, Method for Inviscid Compressible Flows,* NASA Langley Tech. Paper No. 2613, 1986 (unpublished).
5. B. Einefldt, C. D. Munz, P. L. Roe, and B. Sjögreen, On Godunov-type methods near low density, *J. Comput. Phys.* **92** (1991).
6. A. K. Gunstensen, D. H. Rothman, S. Zaleski, and G. Zanetti, Lattice Boltzmann model of immiscible fluids, *Phys. Rev. A* **43**(8), 4320 (1991).
7. S. Harris, *An Introduction to the Theory of the Boltzmann Equation* (Holt, Rinehart, & Winston, New York, 1971).
8. A. Harten, On a class of high resolution total variation stable finite difference schemes, *SIAM J. Numer. Anal.* **21,** 1 (1984).
9. A. Harten, B. Engquist, S. Osher, and S. Chakravarthy, Uniformly high order accurate essentially non-oscillatory schemes, III, *J. Comput. Phys.* **71,** 231 (1987).
10. A. Jameson, Positive schemes and shock modeling for compressible flows, *Int. J. Num. Methods Fluids* **20,** 743 (1995).
11. S. Karni, Multicomponent flow calculations by a consistent primitive algorithm, *J. Comput. Phys.* **112,** 31 (1994).
12. Smadar Karni, Hybrid multifluid algorithms, *SIAM J. Sci. Comput.,* to appear.
13. B. Larrouturou, How to preserve the mass fraction positive when computing compressible multi-component flow, *J. Comput. Phys.* **95,** 59 (1991).
14. S. Osher and J. A. Sethian, Front propagating with curvature-dependent speed: Algorithms based on Hamilton–Jacobi formulations, *J. Comput. Phys.* **79,** 12 (1988).
15. B. Perthame, Second-order Boltzmann schemes for compressible Euler equation in one and two space dimensions, *SIAM J. Numer. Anal.* **29**(1) (1992).
16. K. H. Prendergast and K. Xu, Numerical hydrodynamics from gas-kinetic theory, *J. Comput. Phys.* **109,** 53 (1993).
17. D. I. Pullin, Direct simulation methods for compressible inviscid ideal gas flow, *J. Comput. Phys.* **34,** 231 (1980).
18. R. D. Reitz, One-dimensional compressible gas dynamics calculations using the Boltzmann equations, *J. Comput. Phys.* **42,** 108 (1981).
19. R. H. Sanders and K. H. Prendergast, The possible relation of the three-kiloparsec arm to explosions in the galactic nucleus, in *Astrophysical Journal,* **188,** 1974.
20. X. Shan and H. Chen, Lattice-Boltzmann model for simulating flows with multiple phases and components, *Phys. Rev. E* **47**(3), 1815 (1993).
21. X. Shan and G. Doolen, Multicomponent Lattice-Boltzmann model with interparticle interactions, *J. Stat. Phys.* **81,** 379 (1995).
22. K. Xu, A gas-kinetic scheme for the Euler equations with heat transfer, submitted to *SIAM J. Sci. Comput.* (1997).
23. K. Xu, C. Kim, L. Martinelli, and A. Jameson, BGK-based schemes for the simulation of compressible flow. *Int. J. Comput. Flu. Dyn.* **7,** 213 (1996).
24. K. Xu, L. Martinelli, and A. Jameson, Gas-kinetic finite volume methods, flux-vector splitting and artificial diffusion, *J. Comput. Phys.* **120,** 48 (1995).
25. K. Xu and K. H. Prendergast, Numerical Navier-Stokes solutions from gas-kinetic theory, *J. Comput. Phys.* **114,** 9 (1994).